SCIENCE CHINA
Chemistry

• ARTICLES •
· SPECIAL TOPIC · Electrochemical Power Sources

December 2017 Vol.60 No.12:1546–1553
doi: 10.1007/s11426-017-9125-y

# Surface-engineering enhanced sodium storage performance of $Na_3V_2(PO_4)_3$ cathode via *in-situ* self-decorated conducting polymer route

Jiexin Zhang[1], Tianci Yuan[1], Haiying Wan[2], Jiangfeng Qian[1], Xinping Ai[1], Hanxi Yang[1] & Yuliang Cao[1*]

[1]*Hubei Key Laboratory of Electrochemical Power Sources, College of Chemistry and Molecular Sciences, Wuhan University, Wuhan 430072, China*
[2]*Jincheng Abound Energy Ltd., Jincheng 048000, China*

Received June 29, 2017; accepted August 21, 2017; published online November 20, 2017

The key to the development of sodium ion battery is materials with a high rate capacity and cycle stability. Conducting coating is an efficient approach to improve electrochemical performance. As a case study, the $Na_3V_2(PO_4)_3$@PEDOT composite was prepared through an *in-situ* self-decorated conducting polymer route without further calcination. The $Na_3V_2(PO_4)_3$ electrode with a 7% poly(3,4-ethylenedioxythiophene) (PEDOT) coating can deliver an initial reversible capacity of 100 mA h $g^{-1}$ at 1 cycle, and 82% capacity retention over 200 cycles. The results also show that the $Na_3V_2(PO_4)_3$ electrode without and with a thick PEDOT coating exhibits poor electrochemical performance, indicating that an appropriate coating layer is important for improving electronic conductivity and regulating Na-ion insertion. Therefore, this work offers possibility to promote the electrochemical performance of poor-conducting materials in sodium-ion batteries using an *in-situ* self-decorated conducting polymer.

**PEDOT, $Na_3V_2(PO_4)_3$, surface coating, cathode, sodium ion batteries**

**Citation:** Zhang J, Yuan T, Wan H, Qian J, Ai X, Yang H, Cao Y. Surface-engineering enhanced sodium storage performance of $Na_3V_2(PO_4)_3$ cathode via *in-situ* self-decorated conducting polymer route. *Sci China Chem*, 2017, 60: 1546–1553, doi: 10.1007/s11426-017-9125-y

## 1 Introduction

The rapid development of new energy sources such as solar and wind energy requires efficient energy storage technology [1]. Among the various technologies, Li-ion batteries have attracted much attention because of their high energy-conversion efficiency and long-term life [2,3]. However, the high cost and limited resources of lithium hinder the development of Li-ion batteries for large-scale applications. Therefore, Na-ion batteries (SIBs) are the most promising alternative for large-scale storage applications because of low cost and widespread availability of Na [4,5].

Since the 1980s, a variety of polyanionic materials such as silicates ($A_2MSiO_4$) [6–9], sulfate ($AMSO_4$), [10–12] phosphate ($A_3M_2PO_4$), [13,14] pyrophosphates ($AMP_2O_7$) [15–17] have attracted much attention. Among them, NASICON-type $Na_3V_2(PO_4)_3$ (NVP) received considerable attention [18–21], because of its high reversible capacity of 117 mA h $g^{-1}$ and potential plateau at 3.4 V vs. $Na^+/Na$ corresponding to the redox couple $V^{4+}/V^{3+}$ [22]. Moreover, this material has a good safety standard even at 450 °C for charging status [23]. The sodiation/desodiation behavior of $Na_3V_2(PO_4)_3$ was first studied by Yamaki group [22], but the results were unsatisfactory because of the poor electronic conductivity of phosphate framework. After that, many strategies such as carbon coating [24–26], decreasing the

*Corresponding author (email: ylcao@whu.edu.cn)

particle size [27,28] and doping [29] have been developed to improve the ion transport kinetics.

An improved performance has been achieved for $Na_3V_2(PO_4)_3$ cathodes following these approaches. Chekannikov *et al*. [30] developed $Na_3V_2(PO_4)_3$/C/Ag nanocomposite material using modified Pechini method that can deliver 117.2 mA h $g^{-1}$ reversible capacity at a current of 11 mA $g^{-1}$. Fang *et al*. [31] developed carbon fiber-wrapped $Na_3V_2(PO_4)_3$ using chemical vapor deposition (CVD) method, and this delivered 38 mA h $g^{-1}$ reversible capacity at 500 C and obtained 50% more capacity for an ultralong cycle life of 20000 cycles at 30 C. Rui *et al*. [32] reported a feasible freeze-drying assisted method to obtain NVP/C/rGO nanocomposite with a capacity retention of 64% for a long cycle life of 10000 cycles at 100 C. Therefore, the development of a better conductive matrix is a facile method to improve the electronic conductivity of $Na_3V_2(PO_4)_3$.

Conducting polymers are ideal coating agents because they not only improve the electrical conductivity, but also provide mechanical flexibility [33,34]. Moreover, the original monomer material forms a conductive polymer membrane using an *in-situ* oxidation polymerization method, ensuring the uniformity of coating layer on the surface of the materials. Among the conductive polymers, poly(3,4-ethylenedioxythiophene) (PEDOT) is a commonly used conductive intermediate because of its high electrical conductivity. Therefore, coating of PEDOT on $Na_3V_2(PO_4)_3$ is a simple and desirable approach to improve the electronic conductivity. Kim *et al*. [35] developed PEDOT-coated $Li_3V_2(PO_4)_3$ under mild processing conditions at a low temperature and delivered 110 mA h $g^{-1}$ (more than 80% of its theoretical capacity) at 30 C rate with 97% capacity retention after 100 cycles at 10 C rate without adding any carbon. Lepage *et al*. [36] reported that the conducting polymer/$LiFePO_4$ composite delivers 163 mA h $g^{-1}$ at 0.1 C rate, which is similar to the theoretical capacity of $LiFePO_4$. Because of these advantages, $Na_3V_2(PO_4)_3$@PEDOT composite was prepared for the first time using an *in-situ* self-decorated conducting polymer route that does not require further calcination, and its structural, morphological, and electrochemical properties were also investigated.

## 2 Experimental

### 2.1 Synthesis of materials

#### 2.1.1 Preparation of bare $Na_3V_2(PO_4)_3$

Bare $Na_3V_2(PO_4)_3$ was prepared by ball mixing and subsequent calcination. All the reagents were purchased from Alfa (USA) and used as received without further purification. First, $V_2O_5$, $NH_4H_2PO_4$ and $Na_2CO_3$ were added in a stoichiometric ratio to ethanol in a high-energy ball mixing vial. To reduce $V^{5+}$ to $V^{4+}$, $H_2C_2O_4{\cdot}2H_2O$ ($V_2O_5$:$H_2C_2O_4{\cdot}2H_2O$=1:4, molar ratio) was added during the ball-milling. The mixture was ground for 2 h and dried in an oven at 80 °C for 8 h. Then, the dried precursor was sintered for 8 h at 850 °C in Ar atmosphere to obtain bare $Na_3V_2(PO_4)_3$ (NVP).

#### 2.1.2 Preparation of $Na_3V_2(PO_4)_3$@PEDOT (NVP@PEDOT) composite

NVP@PEDOT was prepared by *in-situ* surface-self-decorated method using oxidized $Na_{3-x}V_2(PO_4)_3$ to evaluate the effect of oxidative polymerization of 3,4-ethylenedioxythiophene (EDOT) monomer on the surface of $Na_3V_2(PO_4)_3$. To partially oxidize $Na_3V_2(PO_4)_3$, $NO_2BF_4$ (97%, Alfa, USA) was used as the oxidizing agent. First, $NO_2BF_4$ and $Na_3V_2(PO_4)_3$ were added to a Schlenk bottle, and then acetonitrile was added. All the reactions were carried out in Ar atmosphere. The product was washed with acetonitrile, affording the oxidized $Na_{3-x}V_2(PO_4)_3$. Then, the oxidized precursor was added into an EDOT monomer solution to initiate the polymerization reaction of EDOT. Finally, $Na_3V_2(PO_4)_3$@PEDOT (NVP@PEDOT) was obtained. The coating content of PEDOT can be controlled by tuning the oxidizing state of NVP using different molar ratios of NVP and $NO_2BF_4$. In this study, two different molar ratios of NVP and $NO_2BF_4$ (5:1 and 5:2) were selected to prepare NVP@PEDOT composites, marked as NVP@PEDOT-1 and NVP@PEDOT-2, respectively.

#### 2.1.3 Preparation of PEDOT

The bare PEDOT was synthesized using a polymerization method in an aqueous medium. First, HCl (37%, 0.1 mL), a dopant, was added into deionized water. Then, EDOT monomer (0.4 mL) was added dropwise into the HCl solution and homogenized for 10 min. Oxidant, $(NH_4)_2S_2O_8$ (0.73 g), was dissolved in 10 mL deionized water and mixed with the above solution. The mixture was reacted for 48 h, producing a navy-blue precipitate. This solid precipitate was filtered, washed with deionized water, and dried at 50 °C for 24 h to obtain the product as a solid.

### 2.2 Material characterization

Scanning electron microscopy (SEM) images were obtained using a Zeiss Merlin Compact instrument (ZEISS Merlin Compact, Germany), and elemental distribution mappings were obtained using an Oxford X-Max$^N$ probe (INCAPentalFETx3, Oxford Instruments, Britain). Transmission electron microscopy (TEM) was performed using a JEM-2010FEF instrument (JEOL, Japan). X-ray diffraction (XRD) data were obtained using a Shimadzu XRD-6000 diffractometer (Japan) with Cu Kα radiation (40 kV, 30 mA). The $2\theta$ range was from 10° to 60° with a scan rate of 2° $min^{-1}$. Micro-Raman spectra were obtained using an Renishaw InVia Raman spectrometer (Renishaw, Britain) with 532 nm radiation in the range of 500–2500 $cm^{-1}$. The

PEDOT content was measured by thermogravimetric analysis using a TGA Q500 instrument (TA instrumens, the United States) under air. Electrochemical impedance spectra (EIS) were obtained using an Autolab PGSTAT 128N (Eco Chemie, Netherlands). X-ray photoelectron spectra (XPS) were measured using an ESCALAB 250Xi (Thermo Scientific, USA) with Al Kα radiation.

### 2.3 Electrochemical measurements

Electrochemical characterizations were carried out using a half-cell, and a homemade Na piece was used as the counter electrode. The NVP@PEDOT electrodes were prepared by mixing active material, acetylene black, and 4% poly(vinyldifluoride) (PVDF) in a *N*-methyl-2-pyrrolidone (DMF) solution in a ratio of 7:2:1 by weight. The area of the electrode was ~1.13 $cm^2$, while the average loading of the entire material was ~1.5 mg $cm^{-2}$.

All the cells were assembled in a glove box filled with argon gas and tested at a constant temperature. The electrolyte was 1 mol $L^{-1}$ $NaClO_4$ dissolved in ethylene carbonate/diethyl carbonate (EC/DEC, 1:1, *v*/*v*). Cyclic voltammetry tests were performed using a CHI 660C electrochemical workstation (ChenHua Instruments Co., China) at a scan rate of 0.1 mV $s^{-1}$ in the range from 2.6 V to 3.8 V. EIS measurements were conducted in the frequency range from 10 mHz to 100 kHz on both bare NVP and NVP@PEDOT electrodes using an AutoLab PGSTAT 128N (Eco Chemie, Netherlands). Before the EIS tests, the electrodes were relaxed for 4 h. Galvanostatic charge/discharge measurements were performed using a LAND cycler (Wuhan Kingnuo Electronic Co., China) in the voltage range 2.0–4.0 V.

## 3 Results and discussion

Surface engineering using an *in-situ* self-decorate conducting polymer on the surface of $Na_3V_2(PO_4)_3$ provides a tight and conductive coating that is beneficial for improving the electrochemical performance of $Na_3V_2(PO_4)_3$. The mechanism of coating is schematically illustrated in Figure 1. Formation of oxidized $Na_{3-x}V_2(PO_4)_3$ using $NO_2BF_4$ as the oxidizing agent easily oxidizes the EDOT monomer, leading to the formation of PEDOT. In the surface-polymerization process, the formation of conducting polymer and Na-ion reinsertion into the $Na_{3-x}V_2(PO_4)_3$ occurred simultaneously, resulting in a uniform coating of PEDOT on the surface of reduced $Na_3V_2(PO_4)_3$. The reactions of NVP@PEDOT composite are summarized below:

$$Na_3V_2(PO_4)_3 + xNO_2BF_4 \rightarrow Na_{3-x}V_2(PO_4)_3 + xNaBF_4 + xNO_2 \quad (1)$$

$$Na_{3-x}V_2(PO_4)_3 + xNa^+ + EDOTs \rightarrow Na_3V_2(PO_4)_3@PEDOT \quad (2)$$

Figure 2 shows the XRD patterns of pure $Na_3V_2(PO_4)_3$ and NVP@PEDOT composites. All the materials have similar patterns, and all Bragg diffraction peaks of the sample can be assigned to the *R*-3*c* space group (2Na in 18e position, 1Na in 6b position), consistent with the literature [20,37]. All the peaks showed good crystallinity, and no impurity was observed in the diffraction patterns, indicating that PEDOT coating and Na reinsertion have no influence on the structure of NVP.

To investigate the PEDOT coating, the morphologies of the materials were characterized by SEM and TEM. As shown in Figure 3(a), the diameter of bare NVP particle is ~500 nm, and the particles adhere to each other. The particles show a smooth surface and clear corners. After the coating of PEDOT (Figure 3(b, c)), the size and shape of materials showed no obvious change, but the surface became rough and wrinkled, proving the coating of PEDOT to a certain degree. With increasing coating content of PEDOT (NVP@PEDOT-2), clearly a polymer film was produced among the particles (Figure 3(c)). The magnified TEM images clearly show the coating of PEDOT in Figures 3(e, f). The sizes of the coating layers of NVP@PEDOT-1 and NVP@PEDOT-2 were ~40 and 80 nm, respectively, and the NVP@PEDOT-2 showed more peeled-off fragments of PEDOT. The elemental mapping spectra in Figure 3(k–m, o–q) show that Na, V, P, C, O, and S elements were distributed homogeneously in particles, indicating the uniform coating of PEDOT. The PEDOT content was measured by TGA under air condition, as shown in Figure 4. The weight perce-

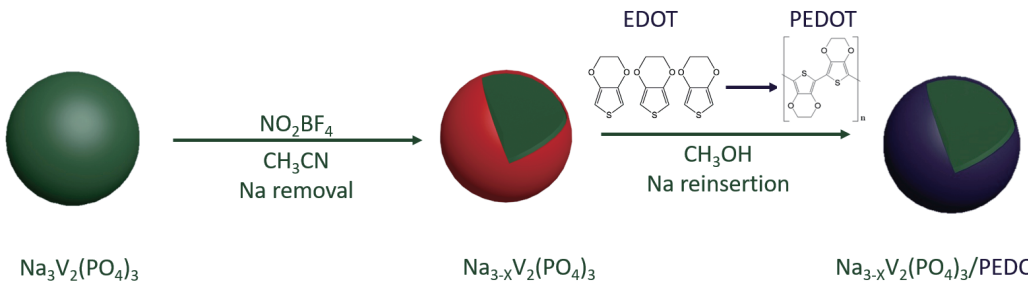


**Figure 1** Schematic illustration of the synthesis of NVP@PEDOT composites (color online).

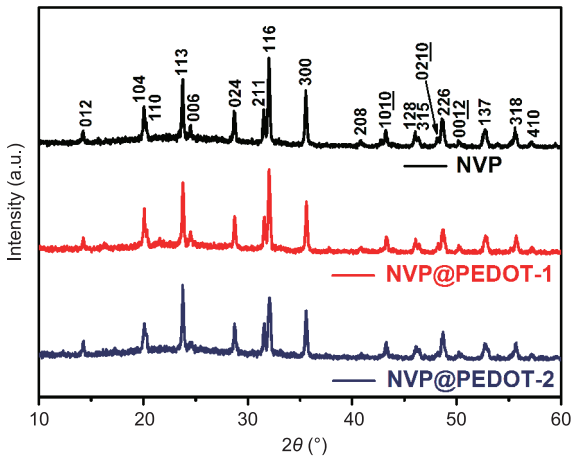


**Figure 2** XRD patterns of NVP and NVP@PEDOT electrodes (color online).

ntage of PEDOT was calculated to be ~7% and 15% for NVP@PEDOT-1 and NVP@PEDOT-2, respectively, according to the weight loss.

To further confirm the existence of PEDOT, its Raman spectra were obtained, as shown in Figure 5. For pure $Na_3V_2(PO_4)_3$ (Figure 5(a)), three peaks corresponding to the stretching vibrations of $PO_4$, $I_D$, and $I_G$ were observed [31]. However, for the coated materials shown in Figure 5(c, d), these peaks cannot be detected, while some typical peaks of PEDOT were observed [38–40]. For instance, the stretching of the symmetric Cα=Cβ(–O) band (1432 $cm^{-1}$), deformation of C–O–C band (1131 $cm^{-1}$), deformation of Cα–S–Cα′ ring (704 $cm^{-1}$), and deformation of oxyethylene ring (578 $cm^{-1}$) are consistent with those for pure PEDOT shown in Figure 3(b).

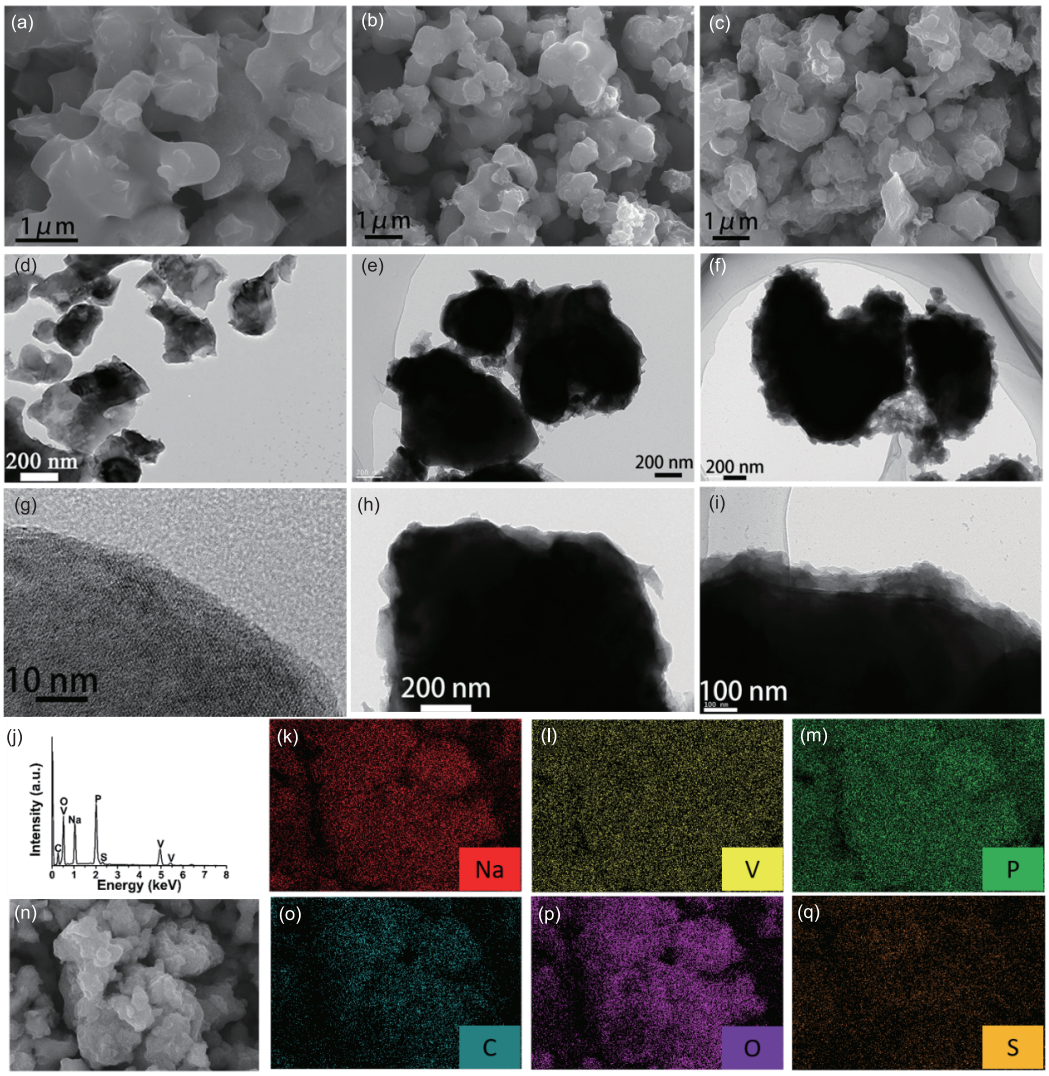


**Figure 3** (a–c) SEM images of NVP, NVP@PEDOT-1 and NVP@PEDOT-2, respectively; (d–f) TEM images of NVP, NVP@PEDOT-1 and NVP@PEDOT-2, respectively; (g–i) magnified TEM images of NVP, NVP@PEDOT-1 and NVP@PEDOT-2, respectively; (j, n) typical EDS and SEM image of NVP@PEDOT-1; (k–m, o–p) the corresponding elemental mapping of (k) sodium (red), (l) vanadium (yellow), (m) phosphorus (green), (o) carbon (cyan), (p) oxygen (purple), and (q) sulfur (orange) (color online).

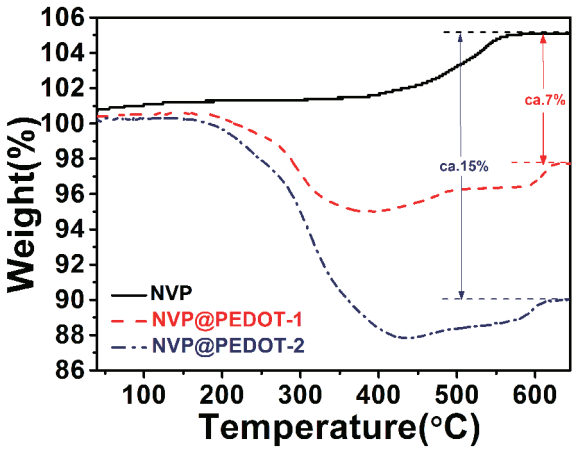


**Figure 4** TG curves of NVP and NVP@PEDOT electrodes (color online).

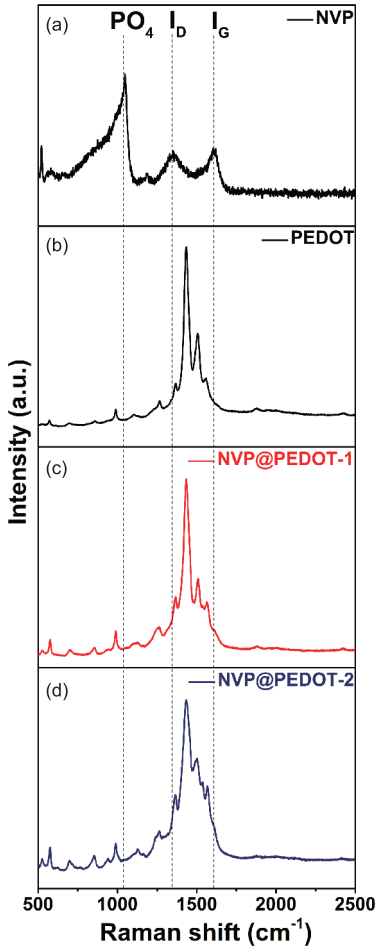


**Figure 5** Raman spectra of NVP (a), PEDOT (b) and NVP@PEDOTs (c, d) electrodes (color online).

Cyclic voltammetry (CV) of bare NVP and NVP@PEDOT composite electrodes were performed in the potential range of 2.8–3.8 V at a scan rate of 0.1 mV $s^{-1}$ as shown in Figure 6(a). One couple of well-defined oxidation and reduction peaks were observed for all the samples, corresponding to reversible $V^{3+/4+}$ redox reaction along with Na-ion insertion and extraction. However, it was clearly observed that the shapes of the oxidation and reduction peaks of NVP@PEDOT electrodes are more symmetrical and sharper than those of bare NVP electrode, indicating a lower polarization and highly reversible electrochemical reaction owing to the conductive coating of PEDOT. Interestingly, NVP@PEDOT-1 exhibited a higher electrochemical reversibility compared to NVP@PEDOT-2 with a high content of PEDOT. This suggests that a thick coating layer could hinder Na-ion diffusion, leading to poor electrochemical properties. Electrochemical performances of NVP@PEDOT composites were investigated in a coin cell using galvanostatic charge/discharge measurement for comparison with the bare NVP electrode. Figure 6(b) shows typical charge/discharge profiles of NVP and NVP@PEDOT electrodes at a current rate of 0.2 C. The NVP@PEDOT-1 electrode showed the highest reversible capacity (105 mA h $g^{-1}$, based on the mass of the NVP@PEDOT) and flattest voltage plateau. However, the charge/discharge profile of bare NVP electrode showed a severe trailing phenomenon, suggesting that the movement of Na ion was suppressed because of low electron conductivity. The result is in good agreement with the CV curve shown in Figure 6(a).

Figure 7(a) shows the rate performances of NVP, NVP@PEDOT-1, and NVP@PEDOT-2 at different current densities (0.1, 0.2, 0.5, 1, 2, 5, 10, 20 and 30 C). The 1 C rate is based on the theoretical capacity of 117 mA h $g^{-1}$, corresponding to 2Na extraction/insertion of $Na_3V_2(PO4)_3$. Both NVP@PEDOT electrodes showed improved capacity and rate performance compared to bare NVP electrode. NVP@PEDOT-1 electrode showed the best electrochemical performance, reaching a reversible capacity of as high as 89, 79, and 58 mA h $g^{-1}$ at high rates of 5, 10 and 20 C, respectively, while the bare NVP electrode only delivered 25, 13, and 5 mA h $g^{-1}$, respectively. This indicates that the coating of PEDOT conducting polymer can efficiently improve the electron conductivity of the material and enhance the electrochemical reversibility of the electrode. When the current was returned to a low rate, the initial capacity of the three electrodes was recovered, exhibiting excellent structural stability. The cycling behaviors of bare NVP and NVP@PEDOT electrodes were also investigated between 2.0–4.0 V as shown in Figure 6(b). NVP@PEDOT-1 electrode delivered a high discharge capacity of 100 mA h $g^{-1}$ at the initial capacity and 93 mA h $g^{-1}$ after 100 cycles at 1 C rate, corresponding to a capacity retention of 93%, while only 89% and 59% for NVP@PEDOT-2 and NVP electrodes, respectively. Even after 200 cycles, NVP@PEDOT-1 electrode exhibited a capacity retention of 82%. The enhanced electrochemical performance of the electrode with PEDOT coating can be

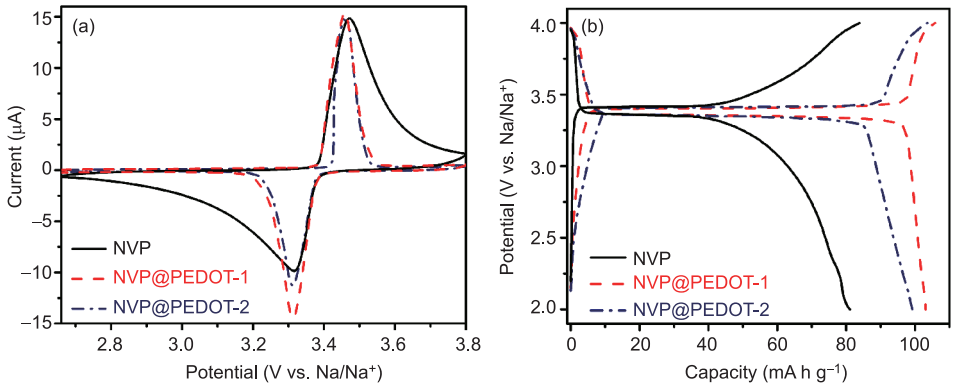


**Figure 6** (a) Cyclic voltammograms of NVP and NVP@PEDOT electrodes at a scan rate of 0.1 mV $s^{-1}$; (b) typical charge/discharge profiles of NVP and NVP@PEDOT electrodes at a current rate of 0.2 C (color online).

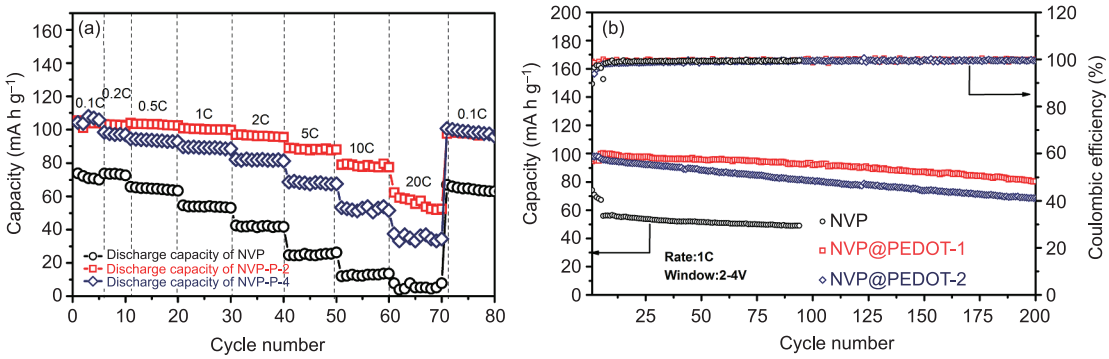


**Figure 7** (a) Rate capability of NVP and NVP@PEDOT electrodes at different current rates; (b) charge/discharge profiles of NVP and NVP@PEDOT electrodes at 1 C rate (color online).

explained as follows: the coated PEDOT improves the electronic conductivity and buffers the structural change during the Na-ion insertion and extraction.

To explain the improved performance by PEDOT coating, EIS analyses of NVP and NVP@PEDOT electrodes were conducted at the discharge state of third cycle. As shown in Figure 8, all the electrodes showed similar Nyquist plots: an oblique line in the low-frequency region and a semicircle in the high-frequency region, corresponding to the Na-diffusion within the bulk phase of the electrode material and charge-transfer impedance ($R_{ct}$) on the electrode/electrolyte interface, respectively. The dynamic parameters of the electrodes were investigated by simulating the experimental result based on the equivalent circuit (inset in Figure 8). Obviously, NVP@PEDOT-1 electrode showed the lowest $R_{ct}$ (850 Ω), indicating the fastest charge-transfer kinetics for Na-ion intercalation.

To further illuminate the electrochemical reaction in the charge/discharge process, XPS was used to investigate the oxidation states of V in the as-prepared, charged, and discharged states shown in Figure 9. The as-prepared material showed a peak located at 516.7 eV, corresponding to $V^{3+}$ [41–43]. Upon charging, the peak increased significantly from its original value to 517.2 eV, indicating the formation of a higher

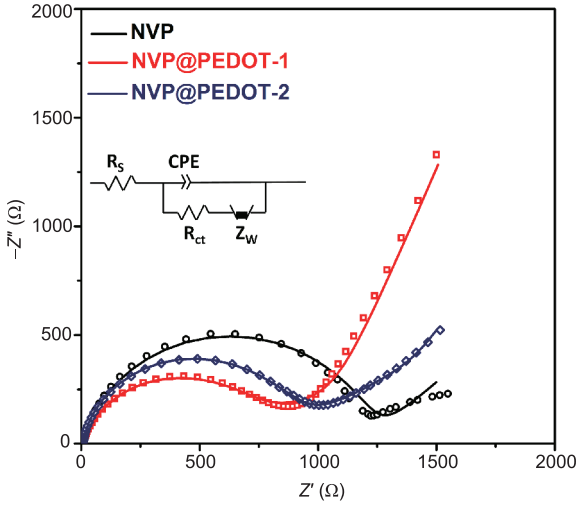


**Figure 8** Electrochemical impedance spectra of NVP and NVP@PEDOT electrodes (color online).

oxidation state ($V^{4+}$) [43,44]. After the discharge, the XPS peak moved back its original value, indicating that the $V^{4+}$ species was completely reduced to $V^{3+}$. The result clearly shows that $2Na^+$ ions can extract/insert reversibly from $Na_3V_2(PO_4)_3$ structure.

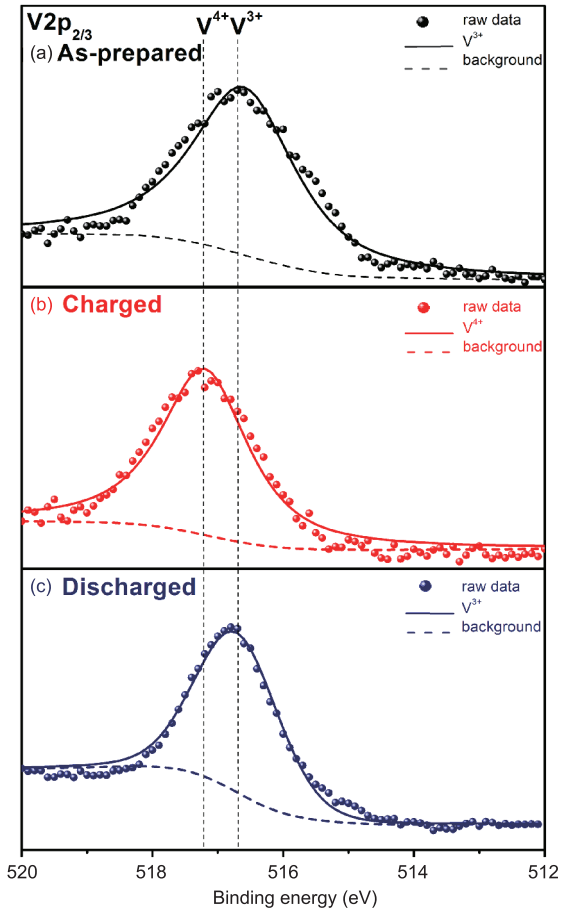


**Figure 9** XPS of NVP and NVP@PEDOT electrodes at the as-prepared (a), charged (b), and discharged (c) states (color online).

## 4 Conclusions

NVP@PEDOT composite was successfully synthesized using the *in-situ* self-decorated method to produce an oxidatively polymerized PEDOT monomer. As a result, the $Na_3V_2(PO_4)_3$ particles were tightly coated with a PEDOT conducting layer. Regarding electrochemical properties, NVP@PEDOT-1 delivered a reversible capacity of 100 mA h $g^{-1}$ at the first cycle and 82% capacity retention after 200 cycles. Both the NVP without PEDOT coating (bare NVP) and with a thick coating film (NVP@PEDOT-2) showed worse electrochemical performances. The better Na storage performance of NVP@PEDOT-1 can be attributed to the PEDOT coating with an appropriate thickness, increasing the electronic conductivity and unhampering the transmission of Na ions in the coating film. The experimental results show that the conducting polymer-coated $Na_3V_2(PO_4)_3$ can be used as a low-cost, high-energy, and long-cycling-life cathode material for the construction of cost-effective Na-ion batteries. This facile self-decorated synthetic method has a potential to achieve an *in-situ* conducting coating on the surface of materials in the energy storage, catalysis, and biomass fields.

**Acknowledgments** This work was supported by the National Key Research Program of China (2016YFB0100400), and the National Natural Science Foundation of China (21373155, 21333007).

**Conflict of interest** The authors declare that they have no conflict of interest.

1 Dunn B, Kamath H, Tarascon JM. *Science*, 2011, 334: 928–935
2 Li H, Wang Z, Chen L, Huang X. *Adv Mater*, 2009, 21: 4593–4607
3 Goodenough JB, Kim Y. *Chem Mater*, 2010, 22: 587–603
4 Palomares V, Casas-Cabanas M, Castillo-Martínez E, Han MH, Rojo T. *Energy Environ Sci*, 2013, 6: 2312
5 Ellis BL, Nazar LF. *Curr Opin Solid State Mater Sci*, 2012, 16: 168–177
6 Guan W, Pan B, Zhou P, Mi J, Zhang D, Xu J, Jiang Y. *ACS Appl Mater Interfaces*, 2017, 9: 22369–22377
7 Li S, Guo J, Ye Z, Zhao X, Wu S, Mi JX, Wang CZ, Gong Z, McDonald MJ, Zhu Z, Ho KM, Yang Y. *ACS Appl Mater Interfaces*, 2016, 8: 17233–17238
8 Chen CY, Matsumoto K, Nohira T, Hagiwara R. *Electrochem Commun*, 2014, 45: 63–66
9 Treacher JC, Wood SM, Islam MS, Kendrick E. *Phys Chem Chem Phys*, 2016, 18: 32744–32752
10 Wei S, Mortemard de Boisse B, Oyama G, Nishimura S, Yamada A. *ChemElectroChem*, 2016, 3: 209–213
11 Barpanda P, Oyama G, Nishimura SI, Chung SC, Yamada A. *Nat Commun*, 2014, 5: 4358–4366
12 Singh P, Shiva K, Celio H, Goodenough JB. *Energy Environ Sci*, 2015, 8: 3000–3005
13 Rajagopalan R, Chen B, Zhang Z, Wu XL, Du Y, Huang Y, Li B, Zong Y, Wang J, Nam GH, Sindoro M, Dou SX, Liu HK, Zhang H. *Adv Mater*, 2017, 29: 1605694
14 Zhu Q, Chang X, Sun N, Liu H, Chen R, Wu F, Xu B. *J Mater Chem A*, 2017, 5: 9982–9990
15 Barpanda P, Ye T, Avdeev M, Chung SC, Yamada A. *J Mater Chem A*, 2013, 1: 4194–4197
16 Kim H, Shakoor RA, Park C, Lim SY, Kim JS, Jo YN, Cho W, Miyasaka K, Kahraman R, Jung Y, Choi JW. *Adv Funct Mater*, 2013, 23: 1147–1155
17 Barpanda P, Liu G, Mohamed Z, Ling CD, Yamada A. *Solid State Ion*, 2014, 268: 305–311
18 Jian Z, Zhao L, Pan H, Hu YS, Li H, Chen W, Chen L. *Electrochem Commun*, 2012, 14: 86–89
19 Jung YH, Lim CH, Kim DK. *J Mater Chem A*, 2013, 1: 11350
20 Saravanan K, Mason CW, Rudola A, Wong KH, Balaya P. *Adv Energy Mater*, 2013, 3: 444–450
21 Zhu C, Song K, van Aken PA, Maier J, Yu Y. *Nano Lett*, 2014, 14: 2175–2180
22 Uebou Y, Kiyabu T, Okada S, Yamaki J-i. The Reports of Institute of Advanced Material Study. Fukuoka: Kyushu University, 2002. 1–5
23 Lim SY, Kim H, Shakoor RA, Jung Y, Choi JW. *J Electrochem Soc*, 2012, 159: A1393–A1397
24 Zhang W, Liu Y, Chen C, Li Z, Huang Y, Hu X. *Small*, 2015, 11: 3822–3829
25 Zhang J, Fang Y, Xiao L, Qian J, Cao Y, Ai X, Yang H. *ACS Appl Mater Interfaces*, 2017, 9: 7177–7184
26 Guo JZ, Wu XL, Wan F, Wang J, Zhang XH, Wang RS. *Chem Eur J*, 2015, 21: 17371–17378
27 Jiang Y, Yang Z, Li W, Zeng L, Pan F, Wang M, Wei X, Hu G, Gu L, Yu Y. *Adv Energy Mater*, 2015, 5: 1402104

28 Li S, Dong Y, Xu L, Xu X, He L, Mai L. *Adv Mater*, 2014, 26: 3545–3553
29 Li H, Yu X, Bai Y, Wu F, Wu C, Liu LY, Yang XQ. *J Mater Chem A*, 2015, 3: 9578–9586
30 Chekannikov A, Kapaev R, Novikova S, Tabachkova N, Kulova T, Skundin A, Yaroslavtsev A. *J Solid State Electrochem*, 2017, 21: 1615–1624
31 Fang Y, Xiao L, Ai X, Cao Y, Yang H. *Adv Mater*, 2015, 27: 5895–5900
32 Rui X, Sun W, Wu C, Yu Y, Yan Q. *Adv Mater*, 2015, 27: 6670–6676
33 Vadivel Murugan A, Muraliganth T, Manthiram A. *Electrochem Commun*, 2008, 10: 903–906
34 Park KS, Schougaard SB, Goodenough JB. *Adv Mater*, 2007, 19: 848–851
35 Kim J, Yoo JK, Jung YS, Kang K. *Adv Energy Mater*, 2013, 3: 1004–1007
36 Lepage D, Michot C, Liang G, Gauthier M, Schougaard SB. *Angew Chem Int Ed*, 2011, 50: 6884–6887
37 Nie P, Zhu Y, Shen L, Pang G, Xu G, Dong S, Dou H, Zhang X. *J Mater Chem A*, 2014, 2: 18606–18612
38 Chiu WW, Travaš-Sejdić J, Cooney RP, Bowmaker GA. *J Raman Spectrosc*, 2006, 37: 1354–1361
39 Selvaganesh SV, Mathiyarasu J, Phani KLN, Yegnaraman V. *Nanoscale Res Lett*, 2007, 2: 546–549
40 Garreau S, Louarn G, Buisson JP, Froyer G, Lefrant S. *Macromolecules*, 1999, 32: 6807–6812
41 Wu CZ, Xie Y, Lei LY, Hu SQ, OuYang CZ. *Adv Mater*, 2006, 18: 1727–1732
42 Chen Q, Wang J, Tang Z, He W, Shao H, Zhang J. *Electrochim Acta*, 2007, 52: 5251–5257
43 Silversmit G, Depla D, Poelman H, Marin GB, De Gryse R. *J Electron Spectrosc Relat Phenom*, 2004, 135: 167–175
44 Conte M, Budroni G, Bartley JK, Taylor SH, Carley AF, Schmidt A, Murphy DM, Girgsdies F, Ressler T, Schlögl R, Hutchings GJ. *Science*, 2006, 313: 1270–1273